Electron Distribution in the Nonclassical Bis(dithiolene) Electron Transfer Series $[M(CO)_2(S_2C_2Me_2)_2]^{0/1-/2-}$ (M = Mo, W): Assessment by Structural, Spectroscopic, and Density Functional Theory Results

Dmitry V. Fomitchev, Booyong S. Lim, and R. H. Holm*

Department of Chemistry and Chemical Biology, Harvard University, Cambridge, Massachusetts 02138

Received September 14, 2000

The electron-transfer series $[M(CO)_2(S_2C_2Me_2)_2]^{0/1-/2-}$ (series 2) have been established, and the previously reported series $[M(S_2C_2Me_2)_3]^{0/1-/2-}$ (series 3) confirmed, by voltammetry (M = Mo, W). Redox reactions are reversible with $E_{Mo} > E_W$, and all members of each series have been isolated. Members of a given series have very similar distorted trigonal prismatic structures; isoelectronic complexes are isostructural. The existence of these series with structurally characterized members facilitates examination of geometric and electronic properties over three consecutive oxidation states. Upon traversing the series in the reducing direction, M−S, S−C, and C−O bond distances increase, and M−C, chelate ring C−C, and ν_{CO} values decrease. Density functional calculations identify the electroactive orbital, which is well separated in energy from other orbitals. Trends in bond lengths and vibrational frequencies in a given series are fully accountable in terms of increasing population of this orbital, whose composition is roughly constant across the series and is dominantly ligand (ca. 80%) in character. Consequently, redox reactions in the two series are essentially ligand-based. The noninnocent nature of dithiolene ligands in oxidized complexes has been long recognized. The results of DFT calculations provide a contemporary description of the delocalized ground states in the two series. The trends in parameters involving the carbonyl groups provide a particularly clear indication of the classical behavior of a π-acceptor ligand in isostructural molecules subject to consecutive reductions over three oxidation states.

Introduction

We have recently utilized the bis(carbonyl)-bis(dithiolene) complexes $[M(CO)_2(S_2C_2R_2)_2]$ (M = Mo, W; R = Me, Ph) as precursors to complexes of potential relevance to the active sites of molybdenum and tungsten enzymes.[1−4] These compounds were first prepared by Schrauzer et al. in 1966,[5] near the beginning of the development of metal dithiolene chemistry and the attendant recognition of dithiolenes as noninnocent ligands. The original preparation involved photolysis of a reaction mixture containing $M(CO)_6$ and $[Ni(S_2C_2R_2)_2]$ in benzene and afforded the products in low yield. By use of $[M(CO)_3(MeCN)_3]$ and stoichiometric reactant ratios, these compounds can now be readily prepared in dichloromethane solution at room temperature without photolysis in improved yields of 30% (M = Mo)[2] and 59−70% (M = W).[1]

Our initial characterization of $[M(CO)_2(S_2C_2R_2)_2]$ complexes has revealed distorted trigonal prismatic stereochemistry for three species[1,2] and the reversible three-member electron-transfer series $[W(CO)_2(S_2C_2Ph)_2]^{0,1-,2-}$.[1] Trigonal prismatic structures of $[M(S_2C_2R_2)_3]^z$ and the multiple redox states $[M(S_2C_2R_2)_2]^z$ and $[M(S_2C_2R_2)_3]^z$ (z = 0, 1−, 2−) are well recognized as defining features of metal dithiolenes.[6−9] Experimental examination of electron delocalization has largely been confined to the S = 1/2 species $[M(S_2C_2R_2)_2]^{1-}$ (M = Ni, Pd, Pt), $[M(S_2C_2R_2)_3]^{1-}$ (M = Mo, W), and $[V(S_2C_2R_2)_3]^{0,2-}$ by analysis of EPR parameters. As is the case for bis- and tris(dithiolenes), nonclassical electron distribution is possible in the $[M(CO)_2(S_2C_2R_2)_2]^z$ set of complexes. For example, limiting formulations of the z = 0 complex are M(IV) with two enedithiolate ligand dianions or M(II) with one enedithiolate dianion and one neutral dithione ligand. Similarly, the doubly reduced complex admits the limiting formulations M(II) with two enedithiolates or M(0) with one enedithiolate and one dithione. The carbonyl groups provide a spectroscopic probe of electron distribution over three molecular oxidation levels that is absent in homoleptic bis- and tris-(dithiolene) systems. For the related complex $[Mo(CO)_2(3,5\text{-}Bu^t_2C_6H_2S_2)_2]$, Sellman et al.[10] have proposed the Mo(IV) state based on carbonyl stretching frequencies.

In this investigation, we have prepared and structurally characterized members of the $[M(CO)_2(S_2C_2Me_2)_2]^{0,1-,2-}$ electron-transfer series with M = Mo and W, and utilized density functional theory to assess electronic structures. To provide a comparison with the more familiar tris(dithiolenes), we have carried out a parallel but less complete investigation of the series $[M(S_2C_2Me_2)_3]^{0,1-,2-}$. The homoleptic six-coordinate series $[V(CNC_6H_3\text{-}2,6\text{-}Me_2)_6]^{1+,0,1-}$ [11] and $[Cr(CNPh)_6]^{0,1+,2+,3+}$ [12] contain ligands related to carbon monoxide. As will be seen, trends

(1) Goddard, C. A.; Holm, R. H. *Inorg. Chem.* **1999**, *38*, 5389.
(2) Lim, B. S.; Donahue, J. P.; Holm, R. H. *Inorg. Chem.* **2000**, *39*, 263.
(3) Sung, K.-M.; Holm, R. H. *Inorg. Chem.* **2000**, *39*, 1275.
(4) Lim, B. S.; Sung, K.-M.; Holm, R. H. *J. Am. Chem. Soc.* **2000**, *122*, 7410.
(5) Schrauzer, G. N.; Mayweg, V. P.; Heinrich, W. *J. Am. Chem. Soc.* **1966**, *88*, 5174.
(6) McCleverty, J. A. *Prog. Inorg. Chem.* **1968**, *10*, 49.
(7) Hoyer, E.; Dietzsch, W.; Schroth, W. *Z. Chem.* **1971**, *11*, 41.
(8) Burns, R. P.; McAuliffe, C. A. *Adv. Inorg. Chem. Radiochem.* **1979**, *22*, 303.
(9) Mahadevan, C. *J. Crystallogr. Spectrosc. Res.* **1986**, 16, 347.
(10) Sellman, D.; Grasser, F.; Knoch, F.; Moll, M. *Angew. Chem., Int. Ed. Engl.* **1991**, *30*, 1311.
(11) Barybin, M. V.; Young, V. G., Jr.; Ellis, J. E. *J. Am. Chem. Soc.* **1998**, *120*, 429.
(12) Bohling, D. A.; Mann, K. R. *Inorg. Chem.* **1984**, *23*, 1426.

10.1021/ic001046w CCC: $20.00
Published on Web 01/13/2001

in certain structural parameters and vibrational frequencies in the $[M(CO)_2(S_2C_2Me_2)_2]^z$ and $[M'(CNAr)_6]^z$ series correlate and support the classical concept of metal bonding to π-acceptor ligands. We are unaware of any other mononuclear metal carbonyls, hetero- or homoleptic, that permit appraisal of structural and vibrational features over an essentially isostructural three-member series of stable molecules.

Experimental Section

Preparation of Compounds. All operations were carried out under strictly anaerobic conditions using either an inert atmosphere box or standard Schlenk techniques. Acetonitrile was freshly distilled from CaH_2; ether and THF were distilled from sodium/benzophenone and stored over 4 Å molecular sieves. The compounds $[M(CO)_2(S_2C_2Me_2)_2]$ (M = Mo,[2] W[1]) and $[M(S_2C_2Me_2)_3]$[13] (M = Mo, W) were prepared by published procedures. Absorption and ^{1}H NMR spectra were determined in acetonitrile solutions unless otherwise noted.

$[Mo(CO)_2(S_2C_2Me_2)_2]$. Absorption spectrum: λ_{max} (ϵ_M) 301 (3630), 393 (6520), 526 (11800), 651 (sh,1060) nm. ^{1}H NMR: δ 2.83.

$[W(CO)_2(S_2C_2Me_2)_2]$. Absorption spectrum: λ_{max} (ϵ_M) 267 (9sh, 5540), 358 (5090), 507 (15300), 640 (749) nm. ^{1}H NMR: δ 2.81.

$[Mo(S_2C_2Me_2)_3]$. Absorption spectrum: λ_{max} (ϵ_M) 258 (sh, 8200), 303 (4210), 436 (14000), 512 (3770), 641 (16800). ^{1}H NMR (C_6D_6): δ 2.25.

$[W(S_2C_2Me_2)_3]$. Absorption spectrum: λ_{max} (ϵ_M) 280 (sh, 4030), 311 (3140), 401 (9920), 508 (3930), 606 (17 740). ^{1}H NMR (C_6D_6): δ 2.24.

$(Et_4N)_2[Mo(CO)_2(S_2C_2Me_2)_2]$. A solution of $K(C_{10}H_{14})$ was prepared from 17 mg (0.44 mmol) of freshly cut potassium and 85 mg (0.44 mmol) of anthracene in 5 mL of THF. The mixture was stirred for 90 min to dissolve the potassium, filtered through Celite, and the filtrate was treated with a solution of 1.18 mg (0.44 mmol) of 18-crown-6 ether in 2 mL of THF. The combined solution was added dropwise with stirring to a magenta solution of 85 mg (0.22 mmol) of $[Mo(CO)_2(S_2C_2Me_2)_2]$ in 3 mL of THF. When the reaction mixture became dark green, a solution of 73 mg (0.44 mmol) of Et_4NCl in 2 mL of acetonitrile was added. The blue-green solid that immediately precipitated was collected by filtration, washed with ether, and dissolved in 4 mL of acetonitrile. The solution was filtered through Celite. Introduction of ether into the filtrate by vapor diffusion over 2 days caused separation of the product as 92 mg (62%) of black needlelike crystals. Absorption spectrum: λ_{max} (ϵ_M) 340 (sh, 4380), 492 (135), 695 (960) nm. ^{1}H NMR: δ 1.94 (v br, anion). Anal. Calcd. for $C_{26}H_{52}MoN_2O_2S_4$: C, 48.13; H, 8.02; N, 4.32; S, 19.78. Found: C, 48.20; H, 7.80; N, 4.28; S, 19.74.

$(Et_4N)[Mo(CO)_2(S_2C_2Me_2)_2]$. A dark green solution of 38 mg (0.059 mmol) of $(Et_4N)_2[Mo(CO)_2(S_2C_2Me_2)_2]$ in 3 mL of acetonitrile was added to a stirred magenta solution of 23 mg (0.059 mmol) of $[Mo(CO)_2(S_2C_2Me_2)_2]$ in 2 mL of THF. A deep blue color appeared instantly. The solution was stirred for 1 h and solvent was removed in vacuo. The black polycrystalline residue was recrystallized from a concentrated acetonitrile solution by vapor diffusion of ether over 4 days. The product was obtained as 33 mg (55%) of black blocklike crystals. Absorption spectrum: λ_{max} (ϵ_M) 295 (sh, 4200), 381 (sh, 2300), 452 (sh, 1200) 594 (sh, 2300), 640 (3000) nm. Anal. Calcd. for $C_{18}H_{32}MoNO_2S_4$: C, 41.68; H, 6.22; N, 2.70; S, 24.73. Found: C, 41.49; H, 6.38; N, 2.69; S, 24.56.

$(Et_4N)_2[W(CO)_2(S_2C_2Me_2)_2]$. This compound was prepared by reduction of $[W(CO)_2(S_2C_2Me_2)_2]$ with $K(C_{10}H_{14})$ in a procedure analogous to the preparation of $(Et_4N)_2[Mo(CO)_2(S_2C_2Me_2)_2]$. The product was isolated as black prismatic crystals (68%); a solution in acetonitrile is bright green. Absorption spectrum: λ_{max} (ϵ_M) 325 (sh, 4150), 370 (sh, 2300), 450 (sh, 950), 630 (920), 710 (sh, 700) nm. ^{1}H NMR: δ 1.97 (br, anion). Anal. Calcd. for $C_{26}H_{52}N_2O_2S_4W$: C, 42.39; H, 7.06; N, 3.80; S, 17.42. Found: C, 41.44; H, 7.23; N, 3.68; S, 17.20.

$(Et_4N)[W(CO)_2(S_2C_2Me_2)_2]$. This compound was prepared by the reaction of $[W(CO)_2(S_2C_2Me_2)_2]$ and $(Et_4N)_2[W(CO)_2(S_2C_2Me_2)_2]$ in a procedure analogous to the preparation of $(Et_4N)[Mo(CO)_2(S_2C_2Me_2)_2]$. The product was obtained as black blocklike crystals (57%); a solution in acetonitrile is deep violet. Absorption spectrum: λ_{max} (ϵ_M) 340 (sh, 3800), 435 (1280), 555 (4350), 608 (4050) nm. Anal. Calcd. for $C_{18}H_{32}NO_2S_4W$: C, 35.64; H, 5.32; N, 2.31; S, 21.15. Found: C, 35.30; H, 4.85; N, 2.32; S, 21.43.

$(Et_4N)_2[Mo(S_2C_2Me_2)_3]$. To a deep green solution of 86 mg (0.19 mmol) of $[Mo(S_2C_2Me_2)_3]$ in 4 mL of acetonitrile was added a solution of 55 mg (0.38 mmol) of $(Et_4N)(BH_4)$ in 2 mL of THF. The reaction mixture immediately became dark green and turned to dark magenta after being stirred for 4 h. Solvent was removed in vacuo to give a dark magenta polycrystalline solid, which was washed with 4 mL of THF and 6 mL of ether and dissolved in 1.5 mL of acetonitrile. The product was obtained as 88 mg (65%) of dark magenta platelike crystals by vapor diffusion of ether into a concentrated acetonitrile solution over 2 d. Absorption spectrum: λ_{max} (ϵ_M) 302 (3290), 415 (5050), 537 (500), 735 (8860) nm. This compound was identified by an X-ray structure determination.

$(Et_4N)[Mo(S_2C_2Me_2)_3]\cdot MeCN$. This compound was prepared by the method for $(Et_4N)_2[Mo(S_2C_2Me_2)_3]$ but with use of equimolar quantitites of $[Mo(S_2C_2Me_2)_3]$ and $(Et_4N)(BH_4)$. The product was obtained as dark gray-green blocklike crystals (67%). Absorption spectrum: λ_{max} (ϵ_M) 309 (10 300), 364 (2390), 413 (3020), 527 (682), 733 (5240). This compound was identified by an X-ray structure determination.

$(Et_4N)_2[W(S_2C_2Me_2)_3]$. This compound was prepared by a method analogous to that for $(Et_4N)_2[Mo(S_2C_2Me_2)_3]$ (71%). Absorption spectrum: λ_{max} (ϵ_M) 262 (15600), 297 (sh, 11000, 331 (9020), 358 (sh, 5200), 529 (8790), 621 (4330), 705 (754) nm. ^{1}H NMR: δ 2.26 (br, anion). Calcd. for $C_{28}H_{58}N_2S_6W$: C, 42.10; H, 7.32; N, 3.51; S, 24.08. Found: C, 42.20; H, 7.22; N, 3.53; S, 23.96.

$(Et_4N)[W(S_2C_2Me_2)_3]\cdot MeCN$. This compound was prepared by a method analogous to that for $(Et_4N)[Mo(S_2C_2Me_2)_3]$. The product was obtained as dark blue blocklike crystals (71%). Absorption spectrum: λ_{max} (ϵ_M) 281 (7580), 310 (sh, 6100), 370 (5210), 466 (3080), 595 (sh, 2900), 667 (5910) nm. Anal. Calcd. for $C_{20}H_{38}NS_6W$: C, 37.22; H, 5.78; N, 3.90; S, 27.02. Found: C, 37.30; H, 5.91; N, 3.20; S, 26.38.

In the sections which follow, complexes are designated as in Chart 1.

Chart 1. Designation of Molybdenum and Tungsten Complexes

$[Mo(CO)_2(S_2C_2Me_2)_2]$	**1**[2,5]
$[Mo(CO)_2(S_2C_2Me_2)_2]^{1-}$	**2**
$[Mo(CO)_2(S_2C_2Me_2)_2]^{2-}$	**3**
$[W(CO)_2(S_2C_2Me_2)_2]$	**4**[1,5]
$[W(CO)_2(S_2C_2Me_2)_2]^{1-}$	**5**
$[W(CO)_2(S_2C_2Me_2)_2]^{2-}$	**6**
$[Mo(S_2C_2Me_2)_3]$	**7**[2,5,13]
$[Mo(S_2C_2Me_2)_3]^{1-}$	**8**[2]
$[Mo(S_2C_2Me_2)_3]^{2-}$	**9**
$[W(S_2C_2Me_2)_3]$	**10**[13,24]
$[W(S_2C_2Me_2)_3]^{1-}$	**11**
$[W(S_2C_2Me_2)_3]^{2-}$	**12**

X-ray Structure Determinations. Structures of the seven compounds in Table 1 were determined. Crystals were obtained by vapor diffusion of ether into anaerobic acetonitrile solutions, and were mounted on glass fibers in paratone oil and cooled in a stream of dinitrogen (−60 °C). Diffraction data were collected with a Siemens (Bruker) SMART CCD area detector system using ω-scans of 0.3°/frame. In all cases, a complete hemisphere of data was collected. Cell parameters were determined using SMART software. The SAINT package was used for integration of data, Lorentz polarization and decay corrections, and merging of the data. Absorption corrections were applied with SADABS. All structures were solved with the heavy atom method; coordinates of metal atoms were determined from Patterson functions and those of the remaining non-hydrogen atoms from subsequent difference Fourier maps. Structures were refined by a full-matrix least-squares method against F^2 with statistical weighting and anisotropic displacement parameters for all non-hydrogen atoms. In the final stages of refinement, hydrogen atoms were added at idealized positions and refined as riding atoms with a uniform value of U_{iso}. All least-squares refinements were done with the SHELXL-97 structure refinement package.

(13) Schrauzer, G. N.; Mayweg, V. P. *J. Am. Chem. Soc.* **1966**, *88*, 3235.

Table 1. Crystallographic Data[a] for Compounds Containing Complexes **2, 3, 5, 6, 9, 11** and **12**

	(Et_4N)[**2**]	$(Et_4N)_2$[**3**]	(Et_4N)[**5**]	$(Et_4N)_2$[**6**]	$(Et_4N)_2$[**9**]	(Et_4N)[**11**]·MeCN	$(Et_4N)_2$[**12**]
formula	$C_{18}H_{32}MoNO_2S_4$	$C_{26}H_{52}MoN_2O_2S_4$	$C_{18}H_{32}NO_2S_4W$	$C_{26}H_{52}N_2O_2S_4W$	$C_{28}H_{58}MoN_2S_6$	$C_{22}H_{41}N_2S_6W$	$C_{28}H_{58}N_2S_6W$
fw	518.63	648.88	606.54	736.79	711.06	709.78	798.97
cryst system	triclinic	monoclinic	monoclinic	monoclinic	monoclinic	monoclinic	monoclinic
space group	$P\bar{1}$	$P2_1/c$	$P2_1/c$	$P2_1/c$	$P2_1/c$	$P2_1/n$	$P2_1/c$
Z	4	4	8	4	4	4	4
a, Å	12.050(1)	14.399(1)	15.035(3)	14.419(1)	15.7148(8)	9.657(1)	15.764(2)
b, Å	14.969(2)	13.873(1)	11.996(2)	13.817(1)	12.7621(7)	23.791(3)	12.692(1)
c, Å	15.078(2)	18.050(2)	26.302(5)	18.079(2)	18.521(1)	13.430(2)	18.482(2)
α (deg)	113.15(1)	90.0	90.0	90.0	90.0	90.0	90.0
β (deg)	107.75(1)	113.35(1)	96.58(3)	113.47(1)	103.52(1)	106.09(1)	104.03(2)
γ (deg)	90.34(1)	90.0	90.0	90.0	90.0	90.0	90.0
V, Å^3	2357.1(4)	3310.5(5)	4712.6(2)	3303.6(4)	3611.6(3)	2964.5(7)	3587.4(6)
d_{calc}, g/cm^3	1.461	1.302	1.710	1.481	1.308	1.590	1.479
μ, mm^{-1}	0.923	0.672	5.269	3.773	0.730	4.333	3.589
θ range, deg	1.49−28.37	1.54−22.50	1.87−28.28	1.54−28.29	1.33−28.28	1.71−22.50	1.33−28.28
GOF(F^2)	1.008	1.004	1.027	1.134	1.009	1.044	1.117
R1[b] (wR2[c]) % for refl with $I > 2\sigma(I)$	3.63 (8.02)	3.44 (7.11)	4.38 (9.90)	3.30 (8.75)	5.46 (12.53)	4.18 (10.38)	4.15 (9.61)

[a] Data collected at 213 K with graphite monochromatized Mo Kα ($\lambda = 0.71071$ Å) radiation. [b] $R1 = \sum||F_o| - |F_c||/\sum|F_o|$. [c] $wR2 = \{\sum[w(F_o^2 - F_c^2)^2/\sum w(F_o^2)^2]\}^{1/2}$.

The asymmetric units contain one ($(Et_4N)_2$[**3**], $(Et_4N)_2$[**6**], $(Et_4N)_2$-[**9**], (Et_4N)[**11**]·MeCN, $(Et_4N)_2$[**12**]), or two ((Et_4N)[**2**], (Et_4N)[**5**]) formula weights. The cation is disordered in the crystal structure of (Et_4N)[**11**]·MeCN. Crystal data and final agreement factors are listed in Table 1. Because of the large quantity of data, selected mean values of bond lengths and angles are given in Tables 4 and 5 instead of individual data. (See paragraph at the end of this article for Supporting Information available.)

Computational Details. All theoretical calculations were based on approximate density functional theory (DFT),[14,15] and were performed using the Amsterdam Density Functional package (ADF).[16] Basis functions, core expansion functions, core coefficients, and fit functions for molybdenum, tungsten, sulfur, carbon, oxygen, and hydrogen atoms were used as provided from database IV of the ADF package. This includes Slater-type orbital (STO) triple-ζ basis sets for molybdenum, tungsten, sulfur, carbon, oxygen, and hydrogen atoms and a single polarization function for the latter four atoms. Core levels of molybdenum (up to 3d) and tungsten (up to 4d) were treated as frozen orbitals. Relativistic effects have been accounted for by the quasi-relativistic treatment,[17] which employs relativistic frozen core potentials in conjunction with the first-order Pauli Hamiltonian. All geometry optimizations are spin-restricted and based on the local density approximations in the parametrization of Vosko, Wilk, and Nusair.[18] Gradient corrections for exchange (Becke[19]) and correlation (Lee−Yang−Parr[20]) effects were also introduced. Geometry optimizations were based on a quasi-Newton approach;[21] starting geometrical parameters were taken from the X-ray structures. EPR g-tensors were computed using an algorithm implemented in ADF,[22] version 1999.02. Calculations were spin-unrestricted and based on optimized geometries and are referenced to the coordinate systems of Figure 1.

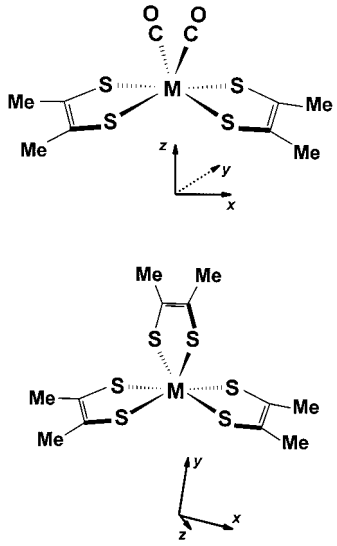

Figure 1. Coordinate system chosen for calculations on **1**−**6** (upper) and **7**−**9** (lower). For the dicarbonyl complexes, the z-axis bisects the C−M−C angle and x-axis passes above the center of the C−C bond of the chelate ring. For the tris(dithiolenes), the z-axis coincides with the molecular C_3 axis and the x-axis passes through the center of one of the chelate ring C−C bonds.

Other Physical Measurements. All measurements were made under anaerobic conditions. Absorption spectra were measured with a Cary 50 Bio spectrophotometer. IR spectra were determined with a Nicolet Nexus 470 FT-IR spectrometer. Electrochemical measurements were performed with a PAR Model 263 potentiostat/galvanostat using a platinum working electrode and 0.1 M $(Bu_4N)(PF_6)$ supporting electrolyte; potentials are referenced to the SCE. EPR spectra were obtained with a Bruker ESP 300E X-band spectrometer equipped with an Oxford Instruments variable temperature accessory and a Hewlett-Packard 5350B frequency counter.

Results and Discussion

Electron Transfer Series. The previously reported neutral complexes **1** and **4** are reduced to dianions **3** and **6**, respectively, with potassium anthracenide in THF and isolated as Et_4N^+ salts. Monoanions **2** and **5** were obtained by redox reaction 1, and were also obtained as Et_4N^+ salts. These

(14) Parr, R. G.; Yang, W. *Density Functional Theory of Atoms and Molecules*; Oxford University Press: Oxford, UK, 1989.
(15) Ziegler, T. *Chem. Rev.* **1991**, *91*, 651.
(16) *The Amsterdam Density Functional program package, v. 1999.02*; the Theoretical Chemistry Group of the Vrije Universiteit in Amsterdam and the Theoretical Chemistry Group of the University of Calgary, Canada, with significant contributions from academic collaborators elsewhere. Baerends, E. J.; Ellis, D. E.; Ros, P. *Chem. Phys.* **1973**, *2*, 41. Versluis, L.; Ziegler, T. *J. Chem. Phys.* **1988**, *88*, 322. te Velde, G.; Baerends, E. J. *Comput. Phys.* **1992**, *99*, 84. Fonseca Guerra, C.; Snijders, J. G.; te Velde, G.; Baerends, E. J. *Theor. Chim. Acta* **1998**, *99*, 391.
(17) (a) Snijders, J. G.; Baerends, E. J.; Ros, P. *Mol. Phys.* **1979**, *38*, 1909. (b) Ziegler, T.; Tschinke, V.; Baerends, E. J.; Snijders, J. G.; Ravenek, W. *J. Phys. Chem.* **1989**, *93*, 3050.
(18) Vosko, S. H.; Wilk, L.; Nusair, M. *Can. J. Phys.* **1980**, *58*, 1200.
(19) Becke, A. D. *Phys. Rev. A* **1988**, *38*, 3098.
(20) Lee, C.; Yang, W.; Parr, R. G. *Phys. Rev. B* **1988**, *372*.
(21) Fan, L.; Ziegler, T. *J. Chem. Phys.* **1991**, *95*, 7401.
(22) van Lenthe, E.; Wormer, P. E. S.; van der Avoird, A. *J. Chem. Phys.* **1997**, *107*, 2488.

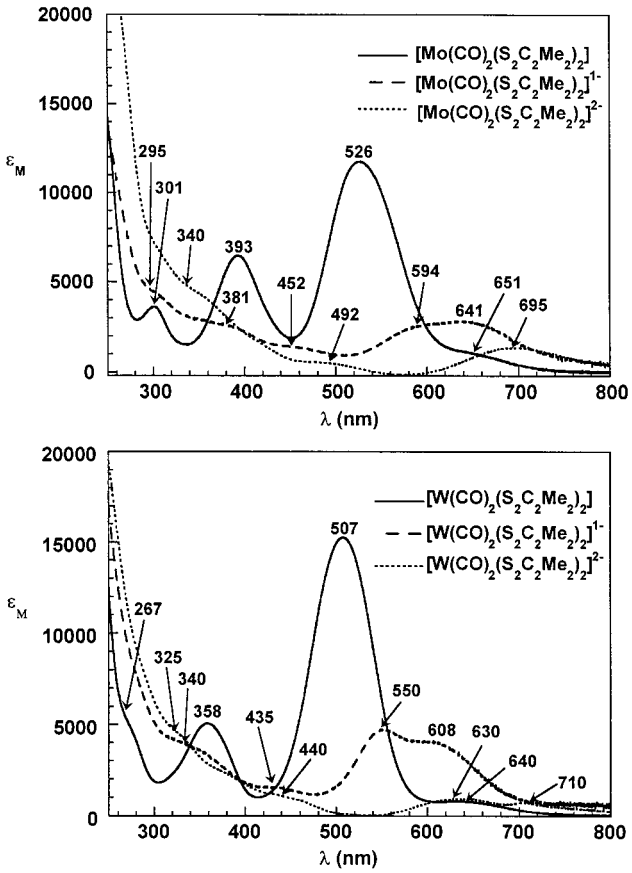

Figure 2. Absorption spectra of the complexes $[M(CO)_2(S_2C_2Me_2)_2]^z$, M = Mo (upper), W (lower), in acetonitrile. Band maxima are indicated.

complexes are most readily recognized by their intense multifeatured UV−visible spectra, which have not been previously reported and are shown in Figure 2. Note that there is a feature-by-feature correspondence in the spectra of isoelectronic complexes. The bands of the tungsten complexes are shifted to

$$[M(CO)_2(S_2C_2Me_2)_2] + [M(CO)_2(S_2C_2Me_2)_2]^{2-} \rightarrow 2[M(CO)_2(S_2C_2Me_2)_2]^{1-} \quad (1)$$

higher energies and, correspondingly, have apparent LMCT character. Complexes **1** and **4** are rendered particularly distinctive by intense bands at 526 and 507 nm, respectively. Intense multifeatured absorption spectra are characteristic of metal dithiolenes, particularly in the more oxidized states.[13,23−25]

As further demonstrated by the voltammograms in Figure 3, complexes **1** and **4** sustain the three-member electron-transfer series 2. At scan rates $v = 10-2000$ mV/s, values of $E_{1/2}$ are independent of scan rate, peak current ratios $i_{pc}/i_{pa} \approx 1$, and plots of $i_p/v^{1/2}$ are linear and independent of v. These properties demonstrate electrochemical reversibility of both steps.[26] Complexes **7** and **10** support the three-member series 3, the existence of which was established much earlier for these and related tris(dithiolenes) of molybdenum and tungsten.[23,27,28] Potentials are summarized in Table 2. For all steps, $E_{Mo} > E_W$, a behavior

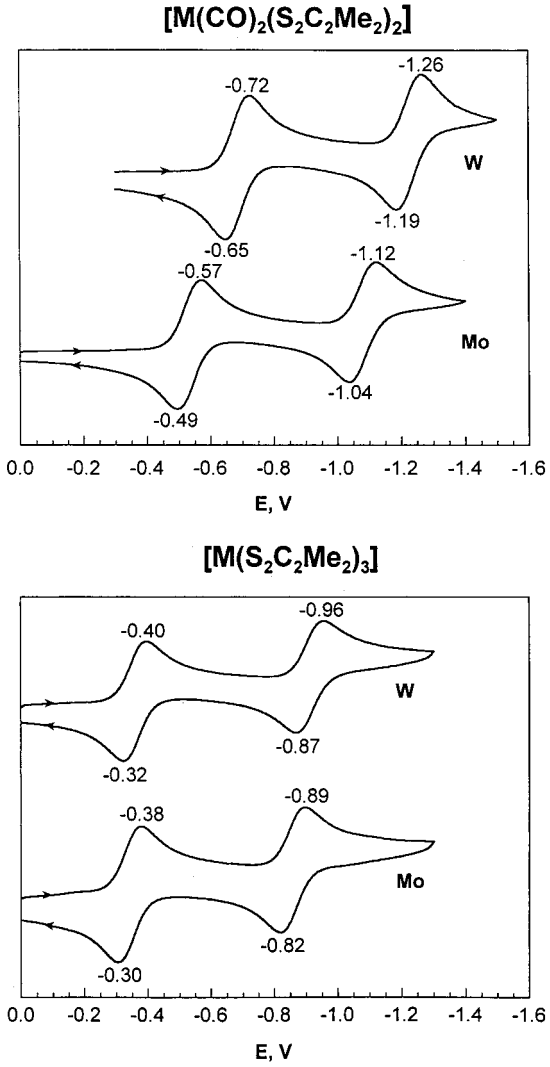

Figure 3. Cyclic voltammograms (100 mV/s) of the electron-transfer series $[M(CO)_2(S_2C_2Me_2)_2]^z$, M = Mo, W; $z = 0, 1-, 2-$ in acetonitrile at ambient temperature. Peak potentials vs SCE are indicated.

always observed at parity of ligands[29−32] and attributed to relativistic effects, which are more pronounced for 5d than 4d

$$[M(CO)_2(S_2C_2Me_2)_2] \leftrightarrow [M(CO)_2(S_2C_2Me_2)_2]^{1-} \leftrightarrow [M(CO)_2(S_2C_2Me_2)_2]^{2-} \quad (2)$$

$$[M(S_2C_2Me_2)_3] \leftrightarrow [M(S_2C_2Me_2)_3]^{1-} \leftrightarrow [M(S_2C_2Me_2)_3]^{2-} \quad (3)$$

orbitals.[33] Many comparative potentials have been tabulated elsewhere.[32] The potential difference $E_{Mo} - E_W$ reaches a maximum for the couples $[MF_6]^{0/1-}$ and $[MF_6]^{1-/2-}$ (ca. 1.0 V),[30] involving well-defined metal oxidation states, and attenuates as the ligand covalency and polarizability increase. The differ-

(23) Wharton, E. J.; McCleverty, J. A. *J. Chem. Soc.* (*A*) **1969**, 2258.
(24) Stiefel, E. I.; Eisenberg, R.; Rosenberg, R. C.; Gray, H. B. *J. Am. Chem. Soc.* **1966**, *88*, 2956.
(25) Sellmann, D.; Zapf, L. *Z. Naturforsch.* **1985**, *40b*, 380.
(26) Brown, E. R.; Large, R. F. In *Physical Methods of Chemistry*; Weissburger, A., Rossiter, B., Eds.; Wiley-Interscience: New York, 1971; Vol. 1, part IIA.
(27) Davison, A.; Edelstein, N.; Holm, R. H.; Maki, A. H. *J. Am. Chem. Soc.* **1964**, *86*, 2799.
(28) Olson, D. C.; Mayweg, V. P.; Schrauzer, G. N. *J. Am. Chem. Soc.* **1966**, *88*, 4876.
(29) Heath, G. A.; Moock, K. A.; Sharp, D. W. A.; Yellowlees, L. J. *J. Chem. Soc., Chem. Commun.* **1985**, 1503.
(30) Moock, K. H.; Heath, G. A. *J. Chem. Soc., Dalton Trans.* **1993**, 2459.
(31) Moock, K. H.; Macgregor, S. A.; Heath, G. A.; Derrick, S.; Boere, R. T. *J. Chem. Soc., Dalton Trans.* **1996**, 2067.
(32) Tucci, G. C.; Donahue, J. P.; Holm, R. H. *Inorg. Chem.* **1998**, *37*, 1602.
(33) Pyykkö, P. *Chem. Rev.* **1988**, *88*, 563.

Table 2. Redox Potentials of Bis- and Tris(dithiolene) Electron Transfer Series in Acetonitrile

		$E_{1/2}$, V[a]	
	z/z−1	M = Mo	M = W
$[M(CO)_2(S_2C_2Me_2)_2]^z$	0/1−	−0.53	−0.69
	1−/2−	−1.08	−1.23
$[M(S_2C_2Me_2)_3]^z$	0/1−	−0.34	−0.36
	1−/2−	−0.86	−0.92

[a] Determined by cyclic voltammetry (100 mV/s) at ~298 K; vs SCE.

Table 3. Infrared Frequencies[a] for the Series $[M(CO)_2(S_2C_2Me_2)_2]^z$

z	M = Mo	M = W
	ν_{CO}[b]	
0	2026, 1962	2023, 1951
1−	1952, 1885	1942, 1865
2−	1875, 1757	1864, 1742
	ν_{CC}	
0	1453 (s)	1472 (m)
1−	1520 (m)	1546 (w)
2−	1586 (vw)	1590 (vw)
	ν_{CS}	
0	931 (m)	930 (m)
1−	925 (w)	926 (w)
2−	901 (w)	901 (vw)

[a] In KBr. [b] All bands vs.

ences in series 2 (160 mV, 150 mV) are larger than in series 3. The values in the latter (20 mV, 60 mV), are among the smallest differences known, a property consistent with the noninnocent character of dithiolene ligands.

Two neutral bis(dithiolene)dicarbonyl[1,2,5] and numerous tris(dithiolene)[5−9,23−25,27,34] complexes have been prepared prior to this work, including members of series 3. For example, the complexes $[M(S_2C_2(CF_3)_2)_3]^{0,1-,2-}$ (M = Cr, Mo, W) have been isolated,[27] but the structures of three members of this set have been determined only recently.[34] There are no previous examples of series 2 and 3 in which all members have been isolated and structurally characterized (with the same ligand). The potential ranges for series 2 (−0.53 to −1.23 V) and 3 (−0.34 to −0.92 V) are neither exceptionally highly oxidizing or reducing, and thus implicate molecules amenable to isolation. In this work, we are concerned with changes in structural and electronic properties as series 2 and 3 are traversed.

Vibrational Frequencies. Values of C−O, chelate ring C−C, and C−S stretching frequencies for series 2 are collected in Table 3. Two ν_{CO} features arise because of cis coordination of the two CO groups in trigonal prismatic stereochemistry (vide infra). Assignments of ν_{CC} and ν_{CS} frequencies are based on previous analyses of the vibrational spectra of dithiolene complexes[35] and molybdoenzymes.[36] As the molybdenum and tungsten complexes become more reduced, ν_{CO} values decrease and the differences between these values increase, consistent with increasing π-back-bonding. The latter trend is in accordance with the Cotton−Kraihanzel prediction that the stretch−stretch interaction constants of a pair of *cis*-carbonyls should increase with increasing π-back-bonding.[37] Values of ν_{CC} increase and ν_{CS} decrease with increased reduction. While these features do not correspond to pure vibrations,[36] the conclusion that emerges is that the dithiolene ligands assume more enedithiolate character as the extent of reduction increases. As will be seen, independent evidence supports this conclusion. Overall, the increased electron density in series 2 is delocalized over both carbonyl and dithiolene ligands. One effect of this delocalization is manifested in the chemical shifts of the diamagnetic members of series 2. In dianions **3** and **6**, the methyl protons are more shielded by 0.8−0.9 ppm than in the neutral complexes **1** and **4**.

Table 4. Selected Mean Bond Lengths (Å) and Angles (deg) for the Series $[M(CO)_2(S_2C_2Me_2)_2]^{0,1-,2-}$(M = Mo, W)

	$[Mo(CO)_2(S_2C_2Me_2)_2]^z$			$[W(CO)_2(S_2C_2Me_2)_2]^z$		
	$z = 0$[a]	$z = 1-$	$z = 2-$	$z = 0$[b]	$z = 1-$	$z = 2-$
	1	**2**	**3**	**4**	**5**	**6**
M−S	2.380(1)	2.408(1)	2.457(1)	2.376(1)	2.406(2)	2.452(1)
M−C	2.025(3)	1.979(5)	1.918(7)	2.030(7)	1.979(7)	1.931(6)
C−O	1.143(4)	1.139(5)	1.179(7)	1.138(10)	1.155(8)	1.175(8)
S−C	1.726(3)	1.745(3)	1.758(5)	1.727(6)	1.747(6)	1.764(6)
C−C[c]	1.367(4)	1.345(5)	1.335(6)	1.366(7)	1.344(8)	1.330(9)
M−C−O	179.1(4)	177.3(4)	177.1(6)	179.0(7)	176.8(6)	176.4(6)
C−M−C	83.5(1)	79.2(2)	72.3(2)	84.1(2)	78.9(4)	72.3(2)
α[d]	144.9	143.8	145.0	144.6	143.1	143.9
θ[e]	131.0	127.5	131.6	132.8	126.3	129.4

[a] Reference 2. [b] Reference 1. [c] Carbon atoms of the dithiolene rings. [d] Mean value of transoid angles, involving S atoms in different chelate rings. [e] Dihedral angle between planes defined by chelate rings, which are nearly planar. Mean MS_2/S_2C_2 dihedral angles in the rings vary from 2.1° (**1**) to 4.5° (**4**).

Structural Trends. The X-ray structures of **2**, **3**, **5**, **6**, **9**, **11**, and **12** were determined in this investigation. Structures of **1**,[2] **4**,[1] **7**,[2] and **8**[2] are available from earlier work; suitable crystals of **10** were not obtained. Selected metric parameters for the two dicarbonyl series are collected in Table 4 and for the tris(dithiolenes) in Table 5. Isoelectronic molybdenum and tungsten complexes are isostructural and essentially isometric. Shape parameters for an octahedron/trigonal prism are the following: transoid angle α = 180°/136° involving atoms in different chelate rings; dihedral angle θ = 90°/120° between planar chelate rings or MS_2 portions if the rings are nonplanar; twist angle φ = 60°/0° between opposite S_3 faces. All members of series 2 and 3 have distorted trigonal prismatic stereochemistry. Further, the members of series 2 approach idealized C_{2v} symmetry with the carbonyl groups in cis positions. This geometry is anticipated by the structures of isoelectronic $[M(bdt)_2L_2]$ (L = RNC, PR_3)[38−40] and $[Mo(3,5\text{-}Bu^t_2bdt)(CO)(PPh_3)]$[10] (bdt = benzene-1,2-dithiolate). The structure of **6**, presented in Figure 4, suffices to represent the structures of **1**−**6**. The structure of **12** in Figure 5 is representative of all members of the tris(dithiolene) series 3. Trigonal prismatic structures or ones intermediate between a trigonal prism and an octahedron are the norm for the molybdenum and tungsten complexes $[M(dithiolene)_3]^{0,1-,2-}$, and have been considered at some length.[34,41−46]

(34) Wang, K.; McConnachie, J. M.; Stiefel, E. I. *Inorg. Chem.* **1999**, *38*, 4334.
(35) Clark, R. J. H.; Turtle, P. C. *J. Chem. Soc., Dalton Trans.* **1978**, 1714.
(36) Garton, S. D.; Hilton, J.; Oku, H.; Crouse, B. R.; Rajagopalan, K. V.; Johnson, M. K. *J. Am. Chem. Soc.* **1997**, *119*, 12906.
(37) Cotton, F. A.; Kraihanzel, C. S. *J. Am. Chem. Soc.* **1962**, *84*, 4432.
(38) Lorber, C.; Donahue, J. P.; Goddard, C. A.; Nordlander, E.; Holm, R. H. *J. Am. Chem. Soc.* **1998**, *120*, 8102.
(39) Donahue, J. P.; Goldsmith, C. R.; Nadiminti, U.; Holm, R. H. *J. Am. Chem. Soc.* **1998**, *120*, 12869.
(40) Lazarowych, N. J.; Morris, R. H. *Can. J. Chem.* **1990**, *68*, 558.
(41) Smith, A. E.; Schrauzer, G. N.; Mayweg, V. P.; Heinrich, W. *J. Am. Chem. Soc.* **1965**, *87*, 5798.
(42) Brown, G. F.; Stiefel, E. I. *Inorg. Chem.* **1973**, *12*, 2140.
(43) Cowie, M.; Bennett, M. J. *Inorg. Chem.* **1976**, *15*, 1584.
(44) Coucouvanis, D.; Hadjikyriacou, A.; Toupadakis, A.; Koo, S.-M.; Ileperuma, O.; Draganjac, M.; Salifoglou, A. *Inorg. Chem.* **1991**, *30*, 754.
(45) Yang, X.; Freeman, G. K. W.; Rauchfuss, T. B.; Wilson, S. R. *Inorg. Chem.* **1991**, *30*, 3034.
(46) Matsubayashi, G.; Douki, K.; Tamura, H.; Nakano, M.; Mori, W. *Inorg. Chem.* **1993**, *32*, 5990.

Table 5. Selected Mean Bond Lengths (Å) and Angles (deg) for the Series $[M(S_2C_2Me_2)_3]^{0,1-,2-}$ (M = Mo, W)

	$[Mo(S_2C_2Me_2)_3]^z$			$[W(S_2C_2Me_2)_3]^z$	
	$z = 0$[a] **7**	$z = 1-$[a] **8**	$z = 2-$ **9**	$z = 1-$ **11**	$z = 2-$ **12**
M−S	2.365(2)[e]	2.375(2)	2.397(2)	2.376(2)	2.389(1)
S−C	1.714(5)	1.725(8)	1.755(5)	1.729(9)	1.758(6)
C−C	1.357(9)	1.354(11)	1.334(8)	1.357(15)	1.326(10)
α[b]	135.4	135.1	134.6	135.4	134.7
θ[c]	119.5−120.8	118.6−121.3	118.5−121.1	119.4−120.5	119.1−120.7
ϕ[d]	3.5[e]	1.6	2.6	2.8	2.4

[a] Reference 2. [b] Transoid angle, involving S atoms in different chelate rings. [c] Range of dihedral angles between MS_2 planes of chelate rings, which in some cases deviate appreciably from planarity. Mean MS_2/C_2S_2 dihedral angles within chelate rings: 15.9° (**7**), 4.0° (**8**), 0.9° (**9**), 7.1° (**11**), 1.0° (**12**). [d] Twist angle between opposite S_3 faces. [e] Incorrectly stated as 2.377(5) Å and 5.4° in ref 2.

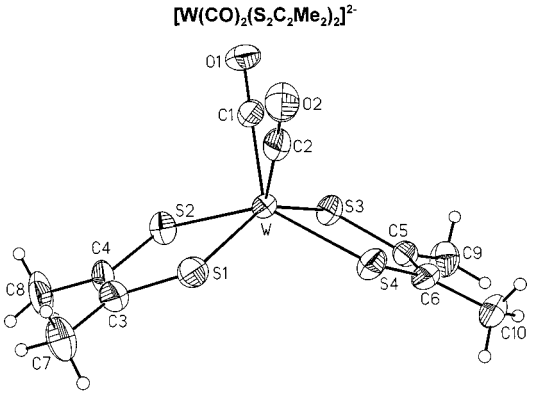

Figure 4. Structure of $[W(CO)_2(S_2C_2Me_2)_2]^{2-}$ as its Et_4N^+ salt showing 50% probability ellipsoids of non-hydrogen atoms and the atom labeling scheme. The structures of complexes **1**−**6** are very similar, as indicated by the parameters in Table 4.

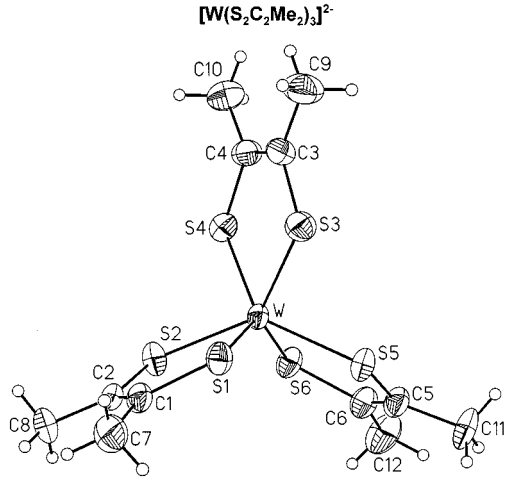

Figure 5. Structure of $[W(S_2C_2Me_2)_3]^{2-}$ as its Et_4N^+ salt showing 50% probability ellipsoids of non-hydrogen atoms and the atom labeling scheme. The structures of complexes **7**−**9**, **11**, and **12** are very similar, as indicated by the parameters in Table 5.

Across the molybdenum and tungsten series 2 and 3 dimensional changes are relatively small, and between adjacent members not always statistically significant, but certain trends do emerge. The bond distances M−S, S−C, and C−O (marginally) increase and M−C and C−C decrease, and the bond angles C−M−C decrease, with increasing reduction. These trends are consistent with the shifts in vibrational frequencies across the series. The changes in M−C and C−O bond distances reflect increased π-back-bonding as the electron count goes up, a matter reflected by decreasing ν_{CO} values across the series. The decreases in the C−M−C angles are suggestive of a weak bonding interaction between the carbonyl ligands. Concerning the chelate rings, bond length changes are indicative of occupation of a molecular orbital which is M−S and S−C antibonding and C−C bonding. For dianions **3**, **6**, **9**, and **12**, S−C and C−C bond lengths are indistinguishable; the values for **3** are 1.758(5) and 1.335(6) Å, respectively. These are in excellent agreement with the typical distances S−C(sp^2) = 1.751(17) Å and (sp^2)C=C(sp^2) = 1.331(9) Å; for comparison, S=C(sp^2) = 1.671(24) Å.[47] The same trend in chelate ring dimensions has been observed in the series $[Ni(S_2C_2Me_2)_2]^{0,1-,2-}$ [48] and for the S−C distance in $[Ni(3,5\text{-}Bu^t_2bdt)_2]^{0,1-,2-}$.[49]

We conclude from spectroscopic and structural results that traversal of series 2 and 3 with M = Mo or W results in largely ligand-based reduction, involving both the carbonyls and dithiolenes in series 2. In the terminal reduced members, the ligand is effectively an enedithiolate dianion; therefore, if an oxidation state were to be assigned it would be M(II) in series 2 and M(IV) in series 3. We examine these conclusions using the results of density functional theory calculations on the members of the two series.

DFT Results. Full geometry optimizations for dicarbonyl complexes **1**−**6** under C_{2v} symmetry and tris(dithiolene) complex **7** under C_s symmetry[50] were carried out. Geometric parameters from the optimized structures of **1**−**7** are collected in Table 6; calculations were not performed on **8**−**12**. The largest discrepancy between experimental and calculated bond lengths is 0.049 Å, and bond angles are calculated to within 1.5°. Trends in bond lengths and angles observed in series 2 and 3 are reproduced, as is evident from the plots in Figure 6 of four bond lengths in the series **1**−**3**. The least satisfactory agreement is with Mo−S bond lengths.

Symmetries and relative energies of the frontier Kohn−Sham orbitals of molybdenum complexes **1**−**3** are given in Figure 7. For the neutral complex **1**, the HOMO is $26a_1$ and the LUMO is $20b_1$. The MO energy level schemes for tungsten complexes **4**−**6** (not shown) are quite similar to those of their molybdenum counterparts, but with larger energy separations between adjacent orbitals. The order of frontier orbitals is unchanged; for neutral **4** the HOMO is $28a_1$ and the LUMO is $22b_1$ owing to the intervention of several lower-lying orbitals with some 4f character. Energy differences between the orbitals $28a_1$ and $22b_1$

(47) Allen, F. H.; Kennard, O.; Watson, D. G.; Brammer, L.; Orpen, A. G.; Taylor, R. In *International Tables of Crystallography*; Volume C, Mathematical, Physical and Chemical Tables; Wilson, A. J. C., Ed.; Kluwer Academic Publishers: Boston, 1995, Sect. 9.5.
(48) Lim, B. S.; Fomitchev, D.; Holm, R. H., results to be published.
(49) Sellmann, D.; Binder, H.; Häussinger, D.; Heinemann, F. W.; Sutter, J. *Inorg. Chim. Acta* **2000**, *300*−*302*, 829. The aromatic character of the bdt ligand dominates to the extent that there is no change in the C−C distances in the chelate rings.
(50) ADF, v. 1999.02, does not admit the idealized C_{3h} symmetry of **7**, which has nonplanar chelate rings. The optimized structure has neglible deviations from C_{3h}.

Table 6. Optimized Geometrical Parameters for the Complexes $[M(CO)_2(S_2C_2Me_2)_2]^z$, $z = 0, 1-, 2-$; M = Mo, W and $[Mo(S_2C_2Me_2)_3]$

	$[Mo(CO)_2(S_2C_2Me_2)_2]^z$			$[W(CO)_2(S_2C_2Me_2)_2]^z$			$[Mo(S_2C_2Me_2)_3]$
	$z = 0$	$z = 1-$	$z = 2-$	$z = 0$	$z = 1-$	$z = 2-$	$z = 0$
	1	**2**	**3**	**4**	**5**	**6**	**7**
M−S	2.396	2.446	2.506	2.374	2.416	2.470	2.384
M−C	2.011	1.971	1.937	1.994	1.959	1.928	
C−O	1.150	1.164	1.180	1.151	1.165	1.182	
S−C	1.713	1.734	1.760	1.715	1.736	1.761	1.714
C−C	1.365	1.353	1.345	1.362	1.350	1.343	1.368
C−C(CH_3)	1.494	1.498	1.498	1.493	1.496	1.496	1.494
M−C−O	178.2	177.6	177.1	178.3	177.7	177.5	
C−M−C	82.2	78.1	73.6	82.7	78.2	73.4	

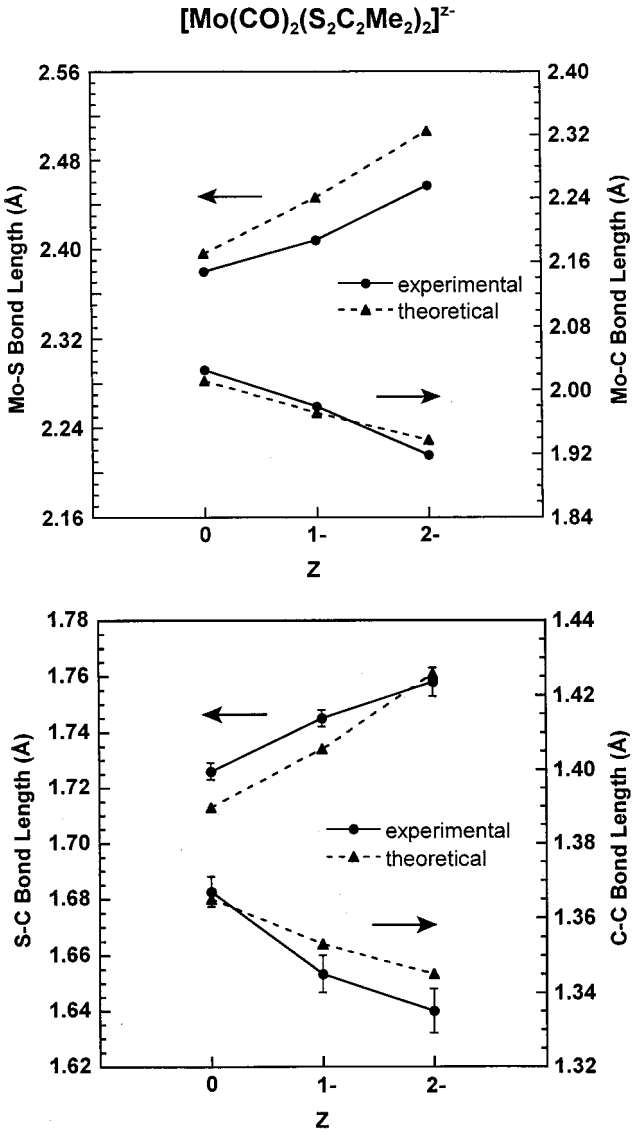

Figure 6. Experimental and theoretical values of bond lengths of $[Mo(CO)_2(S_2C_2Me_2)_2]^{0,1-,2-}$ Upper: Mo−S and Mo−C bonds. Lower: S−C and C−C bonds. In the upper plot the experimental esd's are comparable in size to the markers.

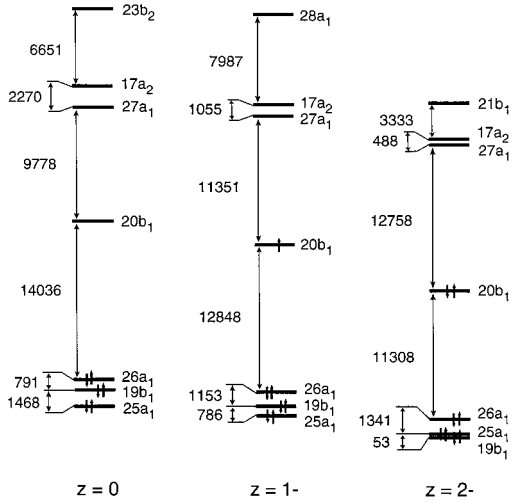

Figure 7. Energy level diagram of $[Mo(CO)_2(S_2C_2Me_2)_2]^{0,1-,2-}$ obtained by DFT calculations. For convenience in plotting, the energy levels of $[Mo(CO)_2(S_2C_2Me_2)_2]^{1-}$ and $[Mo(CO)_2(S_2C_2Me_2)_2]^{2-}$ are shifted by −4 and −8 eV, respectively. Orbital energy separations are given in cm^{-1}.

Table 7. Composition[a] of the $20b_1$ Orbital of $[Mo(CO)_2(S_2C_2Me_2)_2]^{0,1-,2-}$, the $22b_1$ Orbital of $[W(CO)_2(S_2C_2Me_2)_2]^{0,1-,2-}$ and the 55a′ Orbital of $[Mo(S_2C_2Me_2)_3]$

	M	S	C[b]	C[c]	O
	d_{xz}	$p_x + p_y^d + p_z$	$p_x^e + p_z$	π (p_x)	π (p_x)
1	16.3	53.1	17.1	8.2	5.0
2	15.3	54.9	15.6	8.8	5.5
3	15.4	54.7	11.4	9.4	6.4
4	14.6	51.8	17.1	9.8	6.1
5	14.4	53.3	15.2	10.5	6.8
6	15.1	52.3	10.7	11.5	8.2
	Mo	S	C		
	d_{z^2}	$p_x + p_y$	$p_x + p_y$		
7	18.9	54.1	22.8		

[a] Only contributions of more than 1.0% are taken into account. [b] Carbon atoms of the five-member chelate rings. [c] Carbon atoms of the CO groups. [d] Contribution of p_y is <2% of total orbital. [e] Contribution of p_x is <5% of total orbital.

in the tungsten series are 5.5−7.3% larger than differences between the corresponding orbitals $26a_1$ and $20b_1$ in the molybdenum series. Electron-transfer series 2 is enabled by the orbitals $20b_1$ and $22b_1$; these are vacant (LUMO) in **1** and **4**, are singly occupied (SOMO) in **2** and **5**, and are fully occupied (HOMO) in **3** and **6**, respectively. Because of similarities, discussion is confined to molybdenum complexes. Note that $20b_1$ is well separated from the closest occupied MO ($26a_1$) and the next vacant MO ($27a_1$). The composition of orbitals $20b_1$ and $22b_1$ are given in Table 7. These orbitals contain d_{xz} as the only metal component, are highly delocalized and dominantly ligand in character, and change little in composition across the molybdenum and tungsten series 2. In **1**−**3**, for example, the orbitals are 15−16% Mo, 53−55% S, 11−17% ring C, and 13−15% CO. For comparison, the character of filled MO $26a_1$ of these complexes is 25−30% Mo, 29−34% S, 21−34% ring C, and <3% CO. Sections of MO $20b_1$ along different bonds are depicted in Figure 8. These reveal that the orbital is bonding with respect to Mo−C and C−C interactions and antibonding with respect to C−O, Mo−S and S−C interactions. Calculated atom−atom overlap populations based on a Mulliken

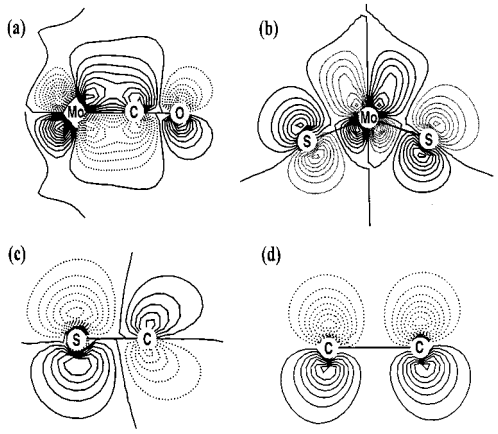

Figure 8. Contour plots showing different sections of MO $20b_1$ of $[Mo(CO)_2(S_2C_2Me_2)_2]$: (a) along the M−C−O bond and perpendicular to the nodal plane; (b) along the S−Mo−S bonds with sulfur atoms belonging to different chelate rings; (c) along the S−C bond and perpendicular to the chelate ring plane; (d) along the chelate ring C−C bond and perpendicular to the chelate ring plane.

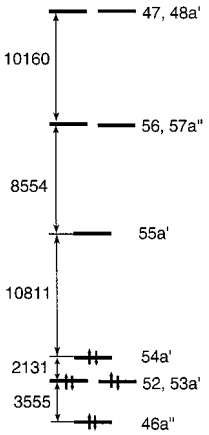

Figure 9. Energy level diagram of $[Mo(S_2C_2Me_2)_3]^0$ obtained by DFT calculations. Orbital energy separations are given in cm^{-1}.

population analysis also reflect trends in ν_{CO} values and bond distances. The following changes in overlap population occur in passing from **1** to **3**: Mo−C, +22%; C−O, −10%; Mo−S, −18%; S−C, −19%, C−C, +13%.

The bonding situation is much the same in the tris(dithiolene)-molybdenum series 3; the energy level diagram for **7** is set out in Figure 9. The electroactive orbital is 55a′, which is well-separated from other orbitals. Throughout the series, this orbital is ca. 80% ligand in character, is composed mainly of sulfur p-orbital contributions (Table 7), and has the same bonding/antibonding properties between adjacent atoms as does MO $20b_1$ in series 2.

We conclude that the trends in vibrational frequencies and bond lengths in series 2 and the latter quantities in series 3 are fully accountable in terms of the DFT orbital energy schemes of Figures 7 and 9. Reduction steps in a given series are predicted to involve the same largely ligand-based orbital whose composition is not strongly altered across a series. The blue-shifted spectra of **4**−**6** vs **1**−**3** are consistent with the larger calculated energy separations between orbitals in the frontier region of the tungsten complexes. The calculations further suggest that the prominent, similarly intense absorptions of $[M(CO)_2(S_2C_2Me_2)_2]$ at 526 and 507 nm, the second lowest-energy features observed (Figure 2), arise from the allowed transitions $19b_1 \rightarrow 20b_1$ (M = Mo) and $21b_1 \rightarrow 22b_1$ (M = W). The apparent LMCT character of these bands noted above is not supported by orbital compositions. For example, the transition $19b_1$ (25%) → $20b_1$ (16%) or an alternative assignment $26a_1$ (22%) → $20b_1$ involve highly delocalized orbitals with minor and roughly constant Mo d-orbital contributions.

Table 8. Experimental[a] and Calculated EPR Parameters

complex		principal values		
$[Mo(CO)_2(S_2C_2Me_2)_2]^{1-}$	g_{exp}	2.027	2.014	2.006
	g_{theor}	2.023	2.020	2.008
	A_{exp} (MHz)[b]	36.9	32.1	44.2
$[W(CO)_2(S_2C_2Me_2)_2]^{1-}$	g_{exp}	2.038	2.019	2.000
	g_{theor}	2.031	2.024	1.997
$[Mo(S_2C_2Me_2)_3]^{1-}$	g_{exp}	2.012	2.012	2.012
$[W(S_2C_2Me_2)_3]^{1-}$	g_{exp}	2.003	1.998	1.987

[a] In DMF/acetonitrile (1:1 v/v) at 5 K. [b] $^{95,97}Mo$.

Bonding analyses at the extended Hückel level have been reported for the diamagnetic complexes $[Mo(CO)_2(S_2CNH_2)_2]$,[51,52] $[Mo(CO)_2(PH_3)_2Cl_2]$,[53] and $[Mo(CO)_2(OMe)_2(py)_2]$,[53] which deviate significantly from octahedral geometry.[54] The complex $[Mo(CO)_2(S_2CNPr^i_2)_2]$ is trigonal prismatic.[51] Although related to **1**−**3** by the presence of a *cis*-$Mo(CO)_2$ fragment, these complexes otherwise contain innocent ligands. Consequently, in these 16-electron molecules frontier orbitals are principally metal in character and the Mo(II) (d^4) description is meaningful.

EPR Spectra. Calculation of the principal components of *g*-tensors serves as an additional check on the reliability of the electronic structure calculations. Here we consider the EPR spectra of the $S = {}^1/_2$ species **2**, **5**, **8**, and **11**. Experimental spectra vary from isotropic to rhombic; *g* values are given in Table 8 and the experimental and simulated spectra of **2** and **5** are available in Figure 10. Metal hyperfine splitting is resolved only in the spectrum of **2**. Results from DFT calculations are in very good agreement with the experimental data (Table 8). The largest discrepancy is 0.007, which compares favorably with differences between experimental *g*-tensor components and values calculated by DFT for $[MOCl_4]^{1-}$ (M = Mo, W) and related d^1 complexes.[55]

All EPR spectra are characterized by average *g* values near $g_e = 2.002$ and small *g* value anisotropy, properties observed for $[M(S_2C_2(CF_3)_2)_3]^{1-}$ (M = Cr, Mo, W),[27] $[V(S_2C_2Ph_2)_3]$,[0,2− 56,57] and related complexes.[23] The spectra could not be interpreted in terms of a M(V) d^1 system in a trigonal ligand field.[27,57] These features together with much reduced metal hyperfine splittings are characteristic of a mainly ligand-based SOMO, as found by DFT for the tris(dithiolene)molybdenum complex **8**. If a metal oxidation state were to be assigned to dicarbonyls **2** and **5**, the obvious choice is M(III) d^3. To our knowledge, there are only two reports on EPR spectra of low-spin Mo(III) complexes, $[Cp^*MoCl_2(PMe_3)_2]$[58] and $[Mo(CN)_7]^{4-}$.[59] In both cases, simulation of the experimental spectra produced distinct principal *g*

(51) Templeton, J. L.; Ward, B. C. *J. Am. Chem. Soc.* **1980**, *102*, 6568.
(52) Templeton, J. L.; Winston, P. B.; Ward, B. C. *J. Am. Chem. Soc.* **1981**, *103*, 7713.
(53) Kubâĉek, P.; Hoffmann, R. *J. Am. Chem. Soc.* **1981**, *103*, 4320.
(54) For an earlier EHMO treatment of alternative octahedral and trigonal prismatic geometries, cf.: Hoffmann, R.; Howell, J. M.; Rossi, A. R. *J. Am. Chem. Soc.* **1976**, *98*, 2484.
(55) Patchkovskii, S.; Ziegler, T. *J. Chem. Phys.* **1999**, *111*, 5730.
(56) Waters, J. H.; Williams, R.; Gray, H. B.; Schrauzer, G. N.; Finck, H. W. *J. Am. Chem. Soc.* **1964**, *86*, 4198.
(57) Davison, A.; Edelstein, N.; Holm, R. H.; Maki, A. H. *Inorg. Chem.* **1965**, *4*, 55.
(58) Baker, R. T.; Morton, J. R.; Preston, K. F.; Williams, A. J.; Le Page, Y. *Inorg. Chem.* **1991**, *30*, 113.
(59) Rossman, G. R.; Tsay, F.-D.; Gray, H. B. *Inorg. Chem.* **1973**, *12*, 824.

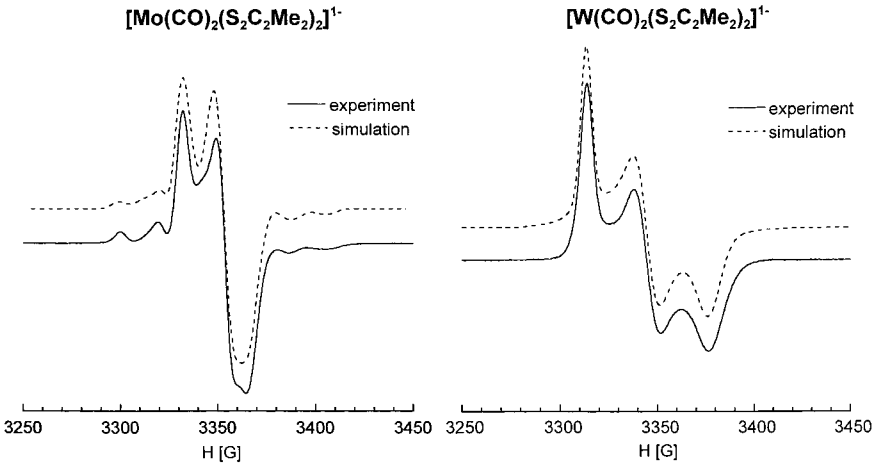

Figure 10. Experimental and simulated X-band EPR spectra of $[Mo(CO)_2(S_2C_2Me_2)_2]^{1-}$ and $[W(CO)_2(S_2C_2Me_2)_2]^{1-}$. Spectra were recorded in DMF/acetonitrile (1:1 v/v) at 5 K.

values with $g_{||} > g_e$ and $g_\perp < g_e$. The spectra of **2** and **5** are rhombic and $g_{exp} \gtrsim g_e$. Further, the slight anisotropy of the *A*-tensor of **2** contrasts with $A_\perp \approx 13A_{||}$ for $[Cp^*MoCl_2(PMe_3)_2]$.[60] If the hyperfine parameters of **2** are analyzed by the formalism of Morton and Preston,[61] we use $A_{||} = 44.2$ MHz and $A_\perp = 34.5$ MHz and recognize that the SOMO has a d_{xz} contribution. The eqs 4 are appropriate, where A_{iso} is the isotropic splitting and *P* is the anisotropic hyperfine parameter ($P_{Mo} = -150.7$ MHz).[61] The difference between the equations gives the expression 5. Depending on the signs of $A_{||}$ and $A_\perp$, the difference is 78.7 or 9.7 MHz. These values do not approach

$$A_{||} = A_{iso} - (4/7)P \qquad A_\perp = A_{iso} + (2/7)P \tag{4}$$

$$A_{||} - A_\perp = -(6/7)P \tag{5}$$

the limiting value of 129.2 MHz for the molybdenum-based electron, and cast considerable doubt on any description of complexes **2** and, by inference, **5** as complexes of Mo(III) and W(III), respectively. The simple argument conforms to the results of the DFT calculations indicating the strongly delocalized nature of the SOMO in these complexes.

Summary. The following are the principal results and conclusions of this investigation.

1. The complexes $[M(CO)_2(S_2C_2Me_2)_2]^{0,1-,2-}$ (M = Mo, W) have been prepared and shown to have distorted trigonal prismatic structures of idealized C_{2v} symmetry. They form the reversible electron-transfer series 2 which exhibits the periodic property $E_{Mo} > E_W$, with $E_{Mo} - E_W = 150$ and 160 mV.

2. The complexes $[M(S_2C_2Me_2)_3]^{0,1-,2-}$ (M = Mo, W) have been prepared and their (slightly) distorted trigonal prismatic structures established. The previously reported reversible electron-transfer series 3 has been confirmed; $E_{Mo} > E_W$ but with $E_{Mo} - E_W = 20$ mV and 60 mV, among the smallest such values known. The relatively small potential differences in series 2 and 3 arise from highly covalent metal−ligand bonding and extensive delocalization of the electrons added in reduction.

3. Series 2 and 3 are the only known sets of metal carbonyl and tris(dithiolene) complexes, respectively, that have been isolated and structurally characterized in three oxidation states. These well-defined series facilitate examination of geometry and electronic structure over three oxidation states.

4. Across series 2 in the reducing direction, a systematic trend in vibrational frequencies and bond distances emerges: ν_{CC}, *d*(M−S), and *d*(S−C) increase, and ν_{CO}, ν_{CS}, *d*(M−C), and *d*(C−C) decrease. The same trend in *d*(M−S), *d*(S−C), and *d*(C−C) is observed in series 3. In the terminal reduced members $[M(CO)_2(S_2C_2Me_2)_2]^{2-}$ (M = Mo, W) and $[Mo(S_2C_2Me_2)_3]^{2-}$, bond distances indicate that the ligand has closely approached or achieved an enedithiolate dianion condition.

5. DFT calculations on the complexes in series 2 (M = Mo, W) and $[Mo(S_2C_2Me_2)_3]$ in series 3 identify the electroactive orbital, which across the series is increasingly occupied, has a nearly constant composition, and is ca. 80% ligand in character. EPR *g* values of $[M(CO)_2(S_2C_2Me_2)_2]^{1-}$ (M = Mo, W) are accurately calculated by DFT. EPR spectra cannot be rationalized in terms of metal-based odd electrons.

6. Frontier orbitals of all members of series 2 and 3 are highly delocalized and electron transfer reactions are largely ligand-based events. The trends in (4) are fully interpretable in terms of the electroactive orbitals specified by DFT.

The noninnocent nature of dithiolene ligands, most pronounced in highly oxidized molecules, has been recognized since the inception of metal dithiolene chemistry.[6,24,27,62−64] This work provides a modern theoretical electronic description that makes extremely clear the delocalized ground-state nature of these complexes, here for members of series 2 and 3. We are inclined to the view that metal oxidation state descriptions in molecules such as $[M(CO)_2(S_2C_2Me_2)_2]^{0,1-}$ and $[M(S_2C_2Me_2)_3]^{0,1-}$ are of questionable heuristic value. Lastly, we observe that the trends in M−C and C−O distances and ν_{CO} values in series 2 are consistent with the classical concept of carbonyl back-bonding. Cases where the effects of bonding to π-acid ligands can be tracked over three oxidation states are uncommon. The homoleptic series $[V(CNC_6H_3\text{-}2,6\text{-}Me_2)_6]^{1+,0,1-}$ [11] and $[Cr(CNPh)_6]^{0,1+,2+,3+}$ [12] cited at the outset are the only other examples known to us. In these series, the M−C distances and ν_{CN} values decrease, and C−N distances increase, with increasing reduction, a behavior paralleled in series 2.

Acknowledgment. This research was supported by NSF Grant CHE 98-76457. We thank Professor M. P. Hendrich (Carnegie Mellon University) for assistance in EPR spectral

(60) Molybdenum hyperfine splitting was not observed for $[Mo(CN)_7]^{4-}$.[59]
(61) Morton, J. R.; Preston, K. F. *J. Magn. Reson.* **1983**, *52*, 457.
(62) Maki, A. H.; Edelstein, N.; Davison, A.; Holm, R. H. *J. Am. Chem. Soc.* **1964**, *86*, 4580.
(63) Schmitt, R. D.; Maki, A. H. *J. Am. Chem. Soc.* **1969**, *90*, 2288.
(64) Schrauzer, G. N. *Acc. Chem. Res.* **1969**, *2*, 72.

simulation, Professor T. Ziegler (University of Calgary) for access to computational facilities and useful discussion, and Dr. S. Patchkovskii (University of Calgary) and Mr. T. Baker (MIT) for assistance with DFT calculations.

Supporting Information Available: X-ray crystallographic files in CIF format for the structure determinations of the seven compounds in Table 1; tables containing molecular orbital energies, occupations, and symmetries for complexes **1**−**9**. This material is available free of charge via the Internet at http://pubs.acs.org.

IC001046W